EUROPEAN SYNCHROTRON RADIATION FACILITY

INSTALLATION EUROPEENNE DE RAYONNEMENT SYNCHROTRON

ESRF

Experiment Report Form

ESRF	**Experiment title:** Elucidating the Lithium Storage Mechanism of Ruthenium-doped Cerium Oxide Anodes via ex situ & operando X-ray Absorption Spectroscopy	**Experiment number**: **A08-1-1107**
Beamline:	**Date of experiment**: from: 21/11/2023 to: 27/11/2023	**Date of report**: 24/12/2023
Shifts: 18	**Local contact(s)**: Alessandro Puri	*Received at ESRF:*

Names and affiliations of applicants (* indicates experimentalists):

*LEPORE Giovanni Orazio - Universita di Firenze Dipartimento di Scienze della Terra

Bresser Dominic, *Xue Xilai, *Li Yunjie - Helmholtz Institut Ulm (HIU) Karlsruher Institut für Technologie (KIT)

Achievements: In this experiment, we successfully collected *ex situ* X-ray absorption spectra (XAS) at the Ce L_{III}-edge, Ru K-edge and Ce K-edge for $Ce_{0.9}Ru_{0.1}O_2$-δ, $Ce_{0.85}Ru_{0.15}O_{2-\delta}$ and carbon-coated $Ce_{0.85}Ru_{0.15}O_{2-\delta}$ in both lithium-ion batteries (LIBs) and sodium-ion batteries (SIBs). *Operando* XANES spectra were measured at the Ru K-edge. Additionally, we acquired XAS spectra at the Ce L_{III}-edge, Sb K-edge and Ce K-edge for $Ce_{0.9}Sb_{0.1}O_{2-\delta}$ to complement the investigation of the role of different metal dopants in the LIBs and SIBs. Spectra at the Ce K-edge and Ce L_{III}-edge were collected in transmission mode, while spectra at the Ru K-edge and Sb K-edge were collected in fluorescence mode. A preliminary analysis of the XANES indicates that: i) The Ce^{4+} undergoes reduction to Ce^{3+} during lithiation, but mostly returns to Ce^{4+} at the fully delithiated state after the 1st and 15th cycle. ii) The Ru dopant is reduced to the near-metallic state during discharge and reverted to Ru^{3+} and Ru $^{4+}$ during the initial charge. However, Ru is gradually reduced to a trivalent state upon cycling. Carbon coating might be involved in the stabilization of the chemical states and local environment of the Ru dopant. iii) For the pristine $Ce_{0.9}Sb_{0.1}O_{2-\delta}$ sample, Sb exhibits an oxidation state close to pentavalent, while Ce is purely tetravalent. During lithiation and sodiation, Sb is reduced to around Sb^{3+}, while it returns to around Sb^{5+} in the fully delithiated and desodiated states.

Report: Graphite is still the anode material of choice for lithium-ion batteries (LIBs), due to its high specific capacity of about 370 mAh g^{-1} and low de-/lithiation potentials of ~0.2 V vs. Li^+/Li. However, the latter in combination with the sluggish kinetics of the lithium intercalation leads to the risk of lithium plating, particularly at high currents.[1] Metal-doped CeO_2 anode materials have been recently reported as a potential substitute – in fact, not only for LIBs, but also for sodium-ion batteries (SIBs), owing to their remarkable electrochemical performance, especially at high currents.[2,3] Among the many possibilities, Fe-doped CeO_2 has been presented as a promising alternative anode for both LIBs and SIBs. Introducing Fe into CeO_2 results in a threefold increase in capacity to more than 300 mAh g^{-1} in LIBs and over 130 mAh g^{-1} in SIBs, compared to non-doped CeO_2, due to the reduction of the Fe dopant to its metallic state and its off-centered position within the crystalline structure.[2,3] Ru shares a comparable electronic structure to Fe, and indeed, (carbon-coated, abbreviated as "cc-") $Ce_{0.85}Ru_{0.15}O_{2-\delta}$ shows a substantially high capacity of over 400 mAh g^{-1} in LIBs, representing the highest initial capacity among all investigated metal-doped CeO_2 anode materials so far. Furthermore, $Ce_{0.85}Ru_{0.15}O_{2-\delta}$ delivered an initial capacity of about 180 mAh g^{-1} in SIBs but suffers from rapid capacity fading. However, the application of a carbon coating resulted in a stabilized capacity of roughly 140 mAh g^{-1}. In addition, the introduction of 10 at-% Sb into CeO_2 yields a stable capacity of 150 mAh g^{-1} in SIBs, yet this improvement is not observed in LIBs, where it only delivers a capacity of 150 mAh g^{-1}. Herein, *ex situ*/*operando* XAS measurements were performed to investigate the impact of different metal dopants in the CeO_2 host structure on the storage mechanism in both LIBs and SIBs.

Figure 1 shows the Ce L_{III}-edge XAS spectra for the Ru-doped CeO_2 samples in LIBs. The XANES spectra at the Ce L_{III}-edge of all presented non-cycled samples substantiate that Ce maintains a comparable local environment. The edge position and the shape of the main absorption edge indicate the presence of Ce^{4+}, and the carbon coating induces a slight reduction in the oxidation state, slightly shifting it to lower than Ce^{4+} (**Figure 1a**). XANES spectra of fully lithiated Ru-doped CeO_2 samples show a reduction from Ce^{4+} to Ce^{3+} (**Figure 1b**). For the delithiated samples, the XANES spectrum of the non-doped CeO_2 sample after 15 cycles shows that the edge position shifts to low energies and the shape looks different compared to the pristine sample, suggesting that the structure might not be stable upon cycling (**Figure 1c**). In the cases of all Ru-doped CeO_2 samples, the shape of the main absorption edge remains comparable before and after the 1st and 15th cycle, which indicates that the Ru dopant stabilizes the CeO_2 host structure during cycling and the doped samples possibly show a higher degree of reoxidation of Ce (**Figure 1d-f**).

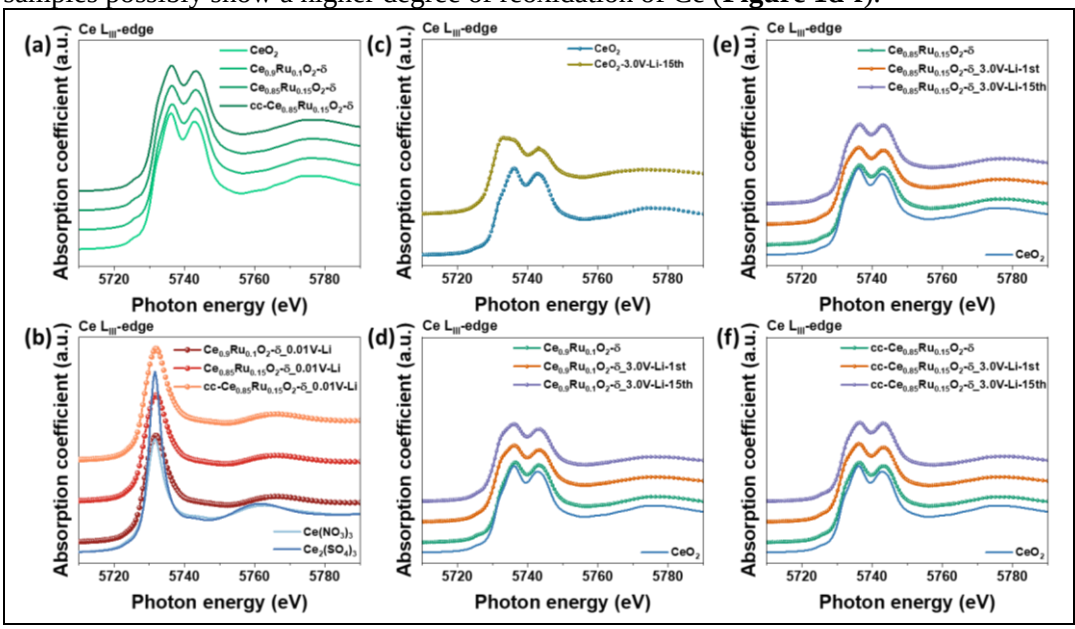

Figure 1. *(a) Ce L_{III}-edge XAS spectra of pristine CeO_2, $Ce_{0.9}Ru_{0.1}O_{2-\delta}$, $Ce_{0.85}Ru_{0.15}O_{2-\delta}$ and cc-$Ce_{0.85}Ru_{0.15}O_{2-\delta}$. (b) Comparison of Ce L_{III}-edge XAS spectra for pristine CeO_2 and recovered electrode at 3.0 V after 15th cycle for LIBs. (c) Comparison of ex situ Ce L_{III}-edge XAS spectra for $Ce_{0.9}Ru_{0.1}O_{2-\delta}$, $Ce_{0.85}Ru_{0.15}O_{2-\delta}$ and carbon-coated $Ce_{0.85}Ru_{0.15}O_{2-\delta}$ electrodes at 0.01 V in the 1st cycle for LIBs. (d-e) Ex situ Ce L_{III}-edge XAS spectra for (d) $Ce_{0.9}Ru_{0.1}O_{2-\delta}$, (e) $Ce_{0.85}Ru_{0.15}O_{2-\delta}$ and (f) cc-$Ce_{0.85}Ru_{0.15}O_{2-\delta}$ electrodes at 3.0 V in the 1st and 15th cycle for LIBs*

Different phenomena in terms of the Ce oxidation states are observed in SIBs, as depicted in **Figure 2**. In both $Ce_{0.85}Ru_{0.15}O_{2-\delta}$ and cc-$Ce_{0.85}Ru_{0.15}O_{2-\delta}$, Ce is not entirely reduced to a trivalent state during sodiation. However, in the fully desodiated state, Ce is in its near-tetravalent state. However, the oxidation state is still lower than that of the pristine sample.

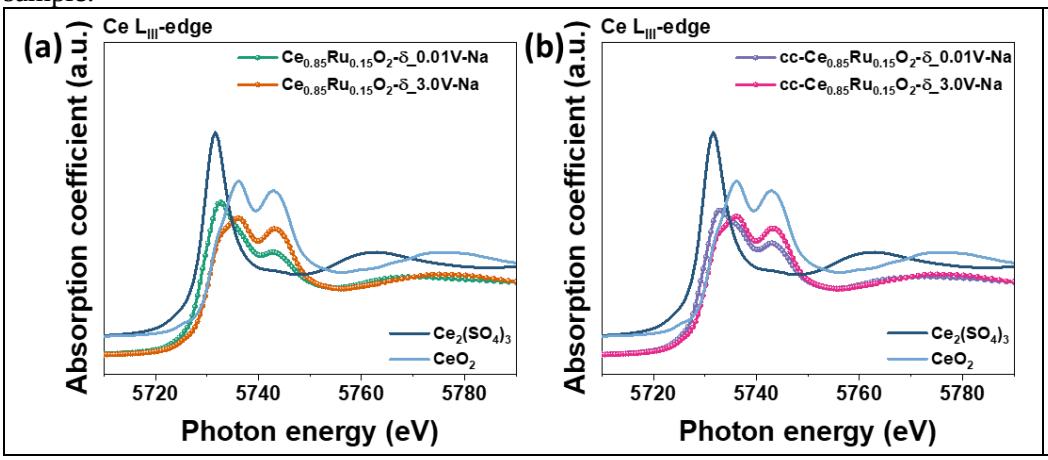

Figure 2. *(a-b) Ex situ Ce L_{III}-edge XAS spectra of (a) $Ce_{0.85}Ru_{0.15}O_{2-\delta}$ and (b) cc-$Ce_{0.85}Ru_{0.15}O_{2-\delta}$ in SIBs.*

Figure 3 presents the Ru-doped CeO_2 XAS data at the Ru K-edge. Typically, their spectral characteristics appear similar, showing Ru in a tetravalent state for all pristine samples. During cycling, the oxidation of Ru is gradually reduced to about trivalent after 15 cycles. The spectra after 15 cycles look different compared to samples before and after the 1st cycle in $Ce_{0.85}Ru_{0.15}O_{2-\delta}$ and $Ce_{0.9}Ru_{0.1}O_{2-\delta}$. In contrast, in the case of cc-$Ce_{0.85}Ru_{0.15}O_{2-\delta}$, the spectral features look more similar between the 1st and 15th cycle, which indicates the structural integrity after initial cycle. Additionally, we performed *operando* XANES measurement with a specific current of 0.1 A g^{-1} for LIBs, allowing for real-time insights into the structural evolution during the whole de-/lithiation process. The *operando* spectra are generally in line with *ex situ* spectra. The edge position and pre-edge shift to lower energies during discharge, indicating the reduction of Ru. During charge, the edge and pre-edge features revert to around Ru^{3+}.

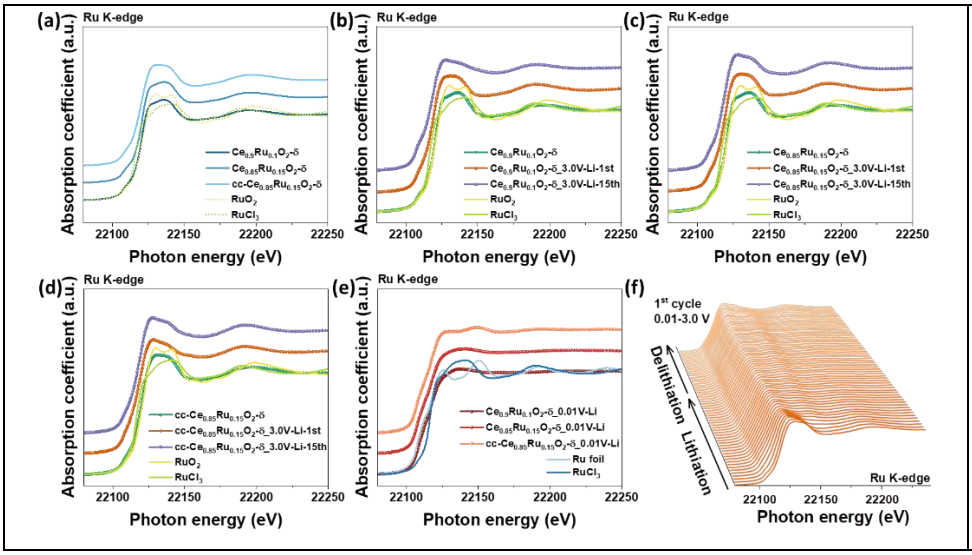

Figure 3. *(a) Ru K-edge XAS spectra of pristine $Ce_{0.9}Ru_{0.1}O_{2-\delta}$, $Ce_{0.85}Ru_{0.15}O_{2-\delta}$ and cc-$Ce_{0.85}Ru_{0.15}O_{2-\delta}$. (b-d) Comparison of ex situ Ru K-edge XAS spectra between 1st and 15th cycle for (b) $Ce_{0.9}Ru_{0.1}O_{2}$-δ, (c) $Ce_{0.85}Ru_{0.15}O_{2-\delta}$ and (d) cc-$Ce_{0.85}Ru_{0.15}O_{2-\delta}$ electrodes at 3.0 V in the 1st for LIBs. (e) Comparison of ex situ Ru K-edge XAS spectra for $Ce_{0.9}Ru_{0.1}O_{2-\delta}$, $Ce_{0.85}Ru_{0.15}O_{2-\delta}$ and cc-$Ce_{0.85}Ru_{0.15}O_{2-\delta}$ electrodes at 0.01 V in the 1st cycle for LIBs. (f) Operando Ru K-edge XANES spectra of cc-$Ce_{0.85}Ru_{0.15}O_{2-\delta}$ during the 1st cycle.*

To investigate the impact of metal doping for electrochemical performance, we also studied $Ce_{0.9}Sb_{0.1}O_{2-\delta}$ samples at the Ce L_{III}-edge and Sb K-edge, **Figure 4** reveals the information about the oxidation states of Ce and Sb. During discharge, Ce^{4+} was reduced to Ce^{3+} in both LIBs and SIBs. However, while Ce recovered to Ce^{4+} in LIBs, it remained mainly Ce^{3+} in SIBs, a distinction not previously observed for other materials for this class. The Sb K-edge spectra show that the oxidation state of Sb for pristine $Ce_{0.9}Sb_{0.1}O_{2-\delta}$ is about Sb^{5+}, and is reduced to around Sb^{3+} during discharge. Additionally, it should be noted that Sb and Ce have a lower oxidation state in SIBs compared to LIBs during discharge.

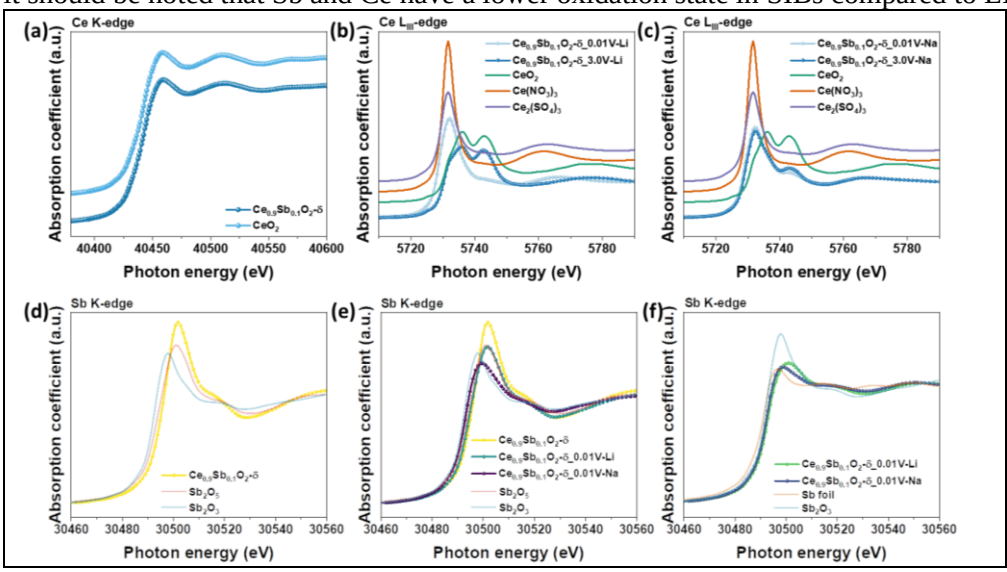

Figure 4. *(a) Ce K-edge XAS spectra of pristine $Ce_{0.9}Sb_{0.1}O_{2-\delta}$. (b-c) Ex situ Ce L_{III}-edge XAS spectra of $Ce_{0.9}Sb_{0.1}O_{2-\delta}$ in (b) LIBs and (c) SIBs. (d-e) Comparison of ex situ Sb K-edge spectra at (d) 0.01 V and (e) 3.0 V in the 1st cycle for LIBs and SIBs.*

To sum up, the preliminary analysis of the *ex situ* XANES data already presents the information on the chemical states, and the evolution of the *operando* spectra at the Ru K-edge is generally in agreement with the *ex situ* experiments. The results show that the ruthenium dopant, indeed, stabilizes the host structure of the CeO_2 during cycling. Further quantitative and in-depth EXAFS analysis for the Ce K-edge and Ru K-edge will unravel the charge storage mechanisms related to the impact of metal doping, which, in turn, advances the development of this class of anode materials based on an advanced insertion-type mechanism. Furthermore, we would like to express our consistent satisfaction with the high-quality spectra collected at the LISA beamline, along with the professionalism of the beamline staff throughout the experiment.

References

[1] J. Asenbauer, T. Eisenmann, M. Kuenzel, A. Kazzazi, Z. Chen, D. Bresser, *Sustain. Energy Fuels* **2020**, *4*, 5387–5416.

[2] Y. Ma, Y. Ma, G. Giuli, H. Euchner, A. Groß, G. O. Lepore, F. d'Acapito, D. Geiger, J. Biskupek, U. Kaiser, H. M. Schütz, A. Carlsson, T. Diemant, R. J. Behm, M. Kuenzel, S. Passerini, D. Bresser, *Adv. Energy Mater.* **2020**, *10*, 202000783.

[3] Y. Ma, Y. Ma, H. Euchner, X. Liu, H. Zhang, B. Qin, D. Geiger, J. Biskupek, A. Carlsson, U. Kaiser, A. Groß, S. Indris, S. Passerini, D. Bresser, *ACS Energy Lett.* **2021**, *6*, 915–924.